



Deposited via The University of Sheffield.

White Rose Research Online URL for this paper:

<https://eprints.whiterose.ac.uk/id/eprint/182753/>

Version: Accepted Version

---

**Article:**

Aldemir Dikici, B., Malayeri, A., Sherborne, C. et al. (2022) Thiolene- and polycaprolactone methacrylate-based polymerized high internal phase emulsion (PolyHIPE) scaffolds for tissue engineering. *Biomacromolecules*, 23 (3). pp. 720-730. ISSN: 1525-7797

<https://doi.org/10.1021/acs.biomac.1c01129>

---

This document is the Accepted Manuscript version of a Published Work that appeared in final form in *Biomacromolecules*, copyright © American Chemical Society after peer review and technical editing by the publisher. To access the final edited and published work see <https://doi.org/10.1021/acs.biomac.1c01129>

**Reuse**

Items deposited in White Rose Research Online are protected by copyright, with all rights reserved unless indicated otherwise. They may be downloaded and/or printed for private study, or other acts as permitted by national copyright laws. The publisher or other rights holders may allow further reproduction and re-use of the full text version. This is indicated by the licence information on the White Rose Research Online record for the item.

**Takedown**

If you consider content in White Rose Research Online to be in breach of UK law, please notify us by emailing [eprints@whiterose.ac.uk](mailto:eprints@whiterose.ac.uk) including the URL of the record and the reason for the withdrawal request.

# Thiolene and polycaprolactone methacrylate-based polymerised high internal phase emulsion (PolyHIPE) scaffolds for tissue engineering

Betül Aldemir Dikici <sup>a, b, c</sup>, Atra Malayeri <sup>a</sup>, Colin Sherborne <sup>a</sup>, Serkan Dikici <sup>a, c</sup>, Thomas Paterson <sup>d</sup>, Lindsey Dew <sup>a</sup>, Paul Hatton <sup>d</sup>, Ilida Ortega Asencio <sup>d</sup>, Sheila MacNeil <sup>a</sup>, Caitlin Langford <sup>e</sup>, Neil R. Cameron <sup>f, g</sup>, Frederik Claeyssens <sup>a, b \*</sup>

<sup>a</sup> Department of Materials Science and Engineering, University of Sheffield, Kroto Research Institute, Sheffield, S3 7HQ, United Kingdom

<sup>b</sup> Department of Materials Science and Engineering, INSIGNEO Institute for In Silico Medicine, University of Sheffield, The Pam Liversidge Building, Sheffield, S1 3JD, United Kingdom

<sup>c</sup> Department of Bioengineering, Izmir Institute of Technology, Urla, Izmir, 35433, Turkey

<sup>d</sup> School of Clinical Dentistry, University of Sheffield, Sheffield, S10 2TA, United Kingdom

<sup>e</sup> Perspectum Diagnostics, Oxford, OX4 2LL, United Kingdom

<sup>f</sup> Department of Materials Science and Engineering, Monash University, 22 Alliance Lane, Clayton, VIC 3800, Australia

<sup>g</sup> School of Engineering, University of Warwick, Coventry CV4 7AL, United Kingdom

\*Corresponding author: [f.claeyssens@sheffield.ac.uk](mailto:f.claeyssens@sheffield.ac.uk)

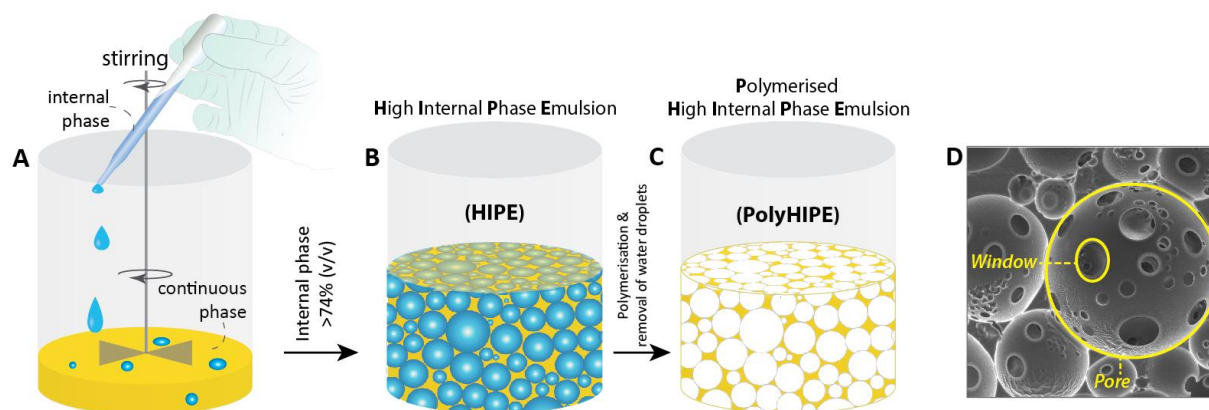
## Abstract:

Highly porous emulsion templated polymers (PolyHIPEs) provide a number of potential advantages in the fabrication of scaffolds for tissue engineering and regenerative medicine. Porosity enables cell ingrowth and nutrient diffusion within - as well as waste removal from - the scaffold. The properties offered by emulsion templating alone include the provision of high interconnected porosity, and - in combination with additive manufacturing - the opportunity to introduce controlled multi-scale porosity to complex or custom structures. However, the majority of monomer systems reported for PolyHIPE preparation are unsuitable for clinical applications as they are non-degradable. Thiol-ene chemistry is a promising route to produce biodegradable photocurable PolyHIPEs for the fabrication of scaffolds using conventional or additive manufacturing methods, however, relatively little research has been reported on this approach. This study reports the groundwork to fabricate a thiol and polycaprolactone (PCL) based PolyHIPE materials via a photoinitiated thiolene click reaction. Two different formulations, either 3-arm PCL methacrylate (3PCLMA) or 4-arm PCL methacrylate (4PCLMA) moieties were used in the PolyHIPE formulation. Biocompatibility of the PolyHIPEs was investigated using human dermal fibroblasts (HDFs) and human osteosarcoma cell line (MG-63) by DNA quantification assay, and developed PolyHIPEs were shown to be capable of supporting cell attachment and viability.

**Keywords:** *emulsion templating, PolyHIPE, polycaprolactone, thiol-ene, tissue engineering, biomaterials, photopolymerisation, porosity*

## 34 1. Introduction

35 A key aspect when producing scaffolds for biomedical applications is the inclusion of interconnected  
36 porosity within the construct; this enables cell ingrowth, nutrient diffusion and waste removal from  
37 the implanted scaffold. Various methods reported to fabricate porous substrates for biomedical  
38 applications include electrospinning<sup>1-3</sup>, 3D printing<sup>4</sup>, and porogen leaching<sup>5,6</sup>. Emulsion templating is  
39 an alternative fabrication route that has gained attention due to its advantages of being (i) tunable,  
40 (ii) providing high porosity (up to 99%) and (iii) interconnectivity (open cellular morphology)<sup>7</sup>. While  
41 an interconnected porous scaffold is important for cell infiltration, tunable chemical, mechanical and  
42 morphological cues enable precise engineering of the substrates for specific biomedical applications.  
43 The principle of emulsion templating is based on creating biphasic emulsions and polymerisation of  
44 the continuous phase (Figure 1). Solidifying of a monomeric continuous phase and subsequent  
45 removal of the internal droplet phase leaves behind a porous structure that is a 3D replica of the initial  
46 emulsion. Emulsions with an internal volume higher than 74% are defined as **High Internal Phase**  
47 **Emulsions (HIPEs)**, and substrates obtained by their polymerisation are called **Polymerised HIPEs**  
48 **(PolyHIPEs)**. To date, there has been a number of significant reviews from the pioneers of the field of  
49 emulsion templating in the literature<sup>8-13</sup>. Also, recently, comprehensive reviews on the development  
50 and use of PolyHIPEs specifically in biomedical applications has been reported<sup>7,14</sup>.



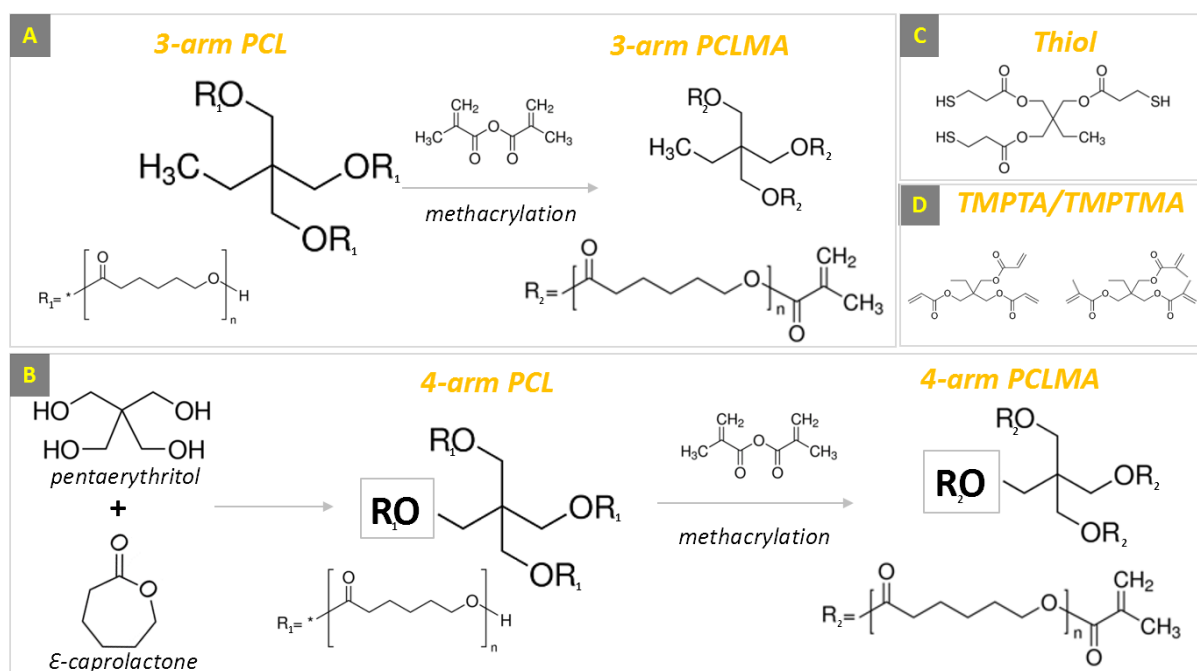
52 **Figure 1:** Fabrication steps of the Polymerised High Internal Phase Emulsion (PolyHIPE). (A, B) The gradual  
53 addition of the internal phase into the continuous phase while the system is mixed, (C) polymerisation of the high  
54 internal phase emulsion (HIPE), (D) scanning electron microscope image of the PolyHIPE (Adapted from<sup>7</sup>).

55 Common monomers reported in PolyHIPE preparations are styrene, its derivatives such as divinyl  
56 benzene (DVB) and acrylate-based monomers, including 2-ethyl-hexyl acrylate (EHA) and isobornyl  
57 acrylate (IBOA)<sup>15-20</sup>. The aforementioned conventional monomers have limited applications for tissue  
58 engineering as they do not degrade within the body.

59 To create a PolyHIPE scaffold often free radical initiated thermal polymerisation is used to set the  
60 monomeric continuous phase into a solid. However, the number of researchers using  
61 photopolymerisation to fabricate PolyHIPE scaffolds has increased <sup>4,15-17,21-28</sup>. Photocuring to produce  
62 PolyHIPEs is a fast and versatile approach; it allows a wide choice of monomers and permits the curing  
63 of less stable emulsions which would otherwise destabilise over the long thermal cure process <sup>22</sup>.

64 There has been an emerging research effort exploring thiol-ene chemistry to produce biodegradable  
65 photocurable PolyHIPEs for tissue engineering applications <sup>26,29,30</sup>. The resulting PolyHIPE material  
66 formed via this chemistry is intended to be fully biodegradable as they are aliphatic polyesters.  
67 Caldwell et al. used a 1:1 trimethylolpropane tris (3-mercaptopropionate) (tri-thiol) and  
68 trimethylolpropane triacrylate (TMPTA) mixture to produce the degradable material <sup>26</sup>. Johnson et al.  
69 showed successful preparation of thiol and triacrylate polycaprolactone (PCL) based PolyHIPE by thiol-  
70 ene click chemistry, which resulted in a fully degradable PolyHIPE material (90% and 95% nominal  
71 porosity) with 60  $\mu\text{m}$  void diameter <sup>30</sup>. Additionally, Susec et al. reported a biocompatible divinyl  
72 adipate and pentaerythritol tetrakis (3-mercaptopropionate) based PolyHIPEs, which they used in a  
73 follow-up study as scaffolds for cartilage repair <sup>21,31</sup>. Recently, Whitely et al. reported on the use of  
74 thiol additives (5-10%) to reduce the oxygen quenching of the radical initiated polymerisation with  
75 negligible change in the properties of the material and biocompatibility of their PolyHIPEs <sup>32</sup>.  
76 Additionally, Langford et al. have shown that thiol-ene based polyHIPEs can be consecutively  
77 functionalised via using the pendant sulphur groups as binding sites via click-chemistry <sup>33</sup>.

78 To summarise, PolyHIPEs have tremendous potential as a scaffold fabrication approach to produce  
79 highly porous biomaterials, where controlled porosity may influence both mass transfer and cell  
80 attachment/migration. However, relatively little progress has been reported in the development of  
81 methods that are ideally suited to the preparation of biocompatible, biodegradable PolyHIPEs with  
82 properties tailored to tissue engineering. PCL has been widely reported as ideally suited for these  
83 applications on account of its excellent biocompatibility and favourable cell response <sup>24,34,35</sup>, and the  
84 aim of this research was, therefore, to investigate a method to prepare thiolene and PCL methacrylate-  
85 based PolyHIPE scaffolds, and evaluate their *in vitro* biocompatibility.



86

87 **Figure 2:** Monomers used in the composition of Thiol-PCL PolyHIPEs. (A) Methacrylate functionalisation of PCL  
 88 triol to obtain 3PCLMA, (B) Synthesis of 4PCL from ring-opening polymerisation of pentaerythritol and  
 89 caprolactone and methacrylate functionalisation. Chemical structures of (C) tri-trithiol and (D) crosslinkers;  
 90 TMPTA/TMPTMA.

## 91 2. Materials and Methods

### 92 2.1. Materials

93 ε-Caprolactone, pentaerythritol, methacrylic anhydride (MAAn), chloroform, toluene, tin 2-  
 94 ethylhexanoate (SnOct<sub>2</sub>), dichloromethane (DCM), triethylamine (TEA) isopropanol,  
 95 trimethylolpropane tris (3-mercaptopropionate) (thiol), trimethylolpropane triacrylate (TMPTA),  
 96 trimethylolpropane trimethacrylate (TMPTMA), diphenyl (2,4,6-trimethyl benzoyl) phosphine  
 97 oxide/2-hydroxy-2-methylpropiophenone blend (photoinitiator), 1,2-Dichloroethane (DCE),  
 98 polycaprolactone triol (M<sub>n</sub> 900 g/mol), Dulbecco's Modified Eagle Media (DMEM), amphotericin B,  
 99 fetal calf serum (FCS), penicillin/streptomycin (PS), L-glutamine, trypsin, paraformaldehyde, resazurin  
 100 sodium salt, MTT, ethanol, DAPI and Phalloidin were all purchased from Sigma Aldrich. Hypermer B246  
 101 (surfactant) was donated by Croda Ltd.

### 102 2.2. Synthesis of 3PCLMA

103 The PCL triol was methacrylate functionalised to obtain 3PCLMA (Figure 2A). First, PCL triol  
 104 (M<sub>n</sub> 900 g/mol, 1 molar equivalent) was dissolved in DCM. TEA (6 molar equivalent) was dissolved in  
 105 50 mL DCM was added to the solution. The mixture was cooled by submerging in a salted ice bath for

106 30 minutes. MAAn (6 molar equivalent) was dissolved in 50 mL DCM and was added dropwise using a  
107 dropping funnel. When MAAn was completely dispensed, the solution was allowed to warm up slowly  
108 to room temperature (RT) and was left to react for 24 hours while covered in foil. Almost all solvent  
109 was removed using a rotary evaporator, and the polymer was purified three times by precipitation  
110 from methanol at -80°C.

### 111 2.3. Synthesis of 4PCLMA

112 The synthesis of 4PCLMA was described in detail in other studies <sup>2,23,24,36,37</sup>. Briefly, 4PCL was  
113 synthesised via ring-opening polymerisation of ε-caprolactone and multifunctional alcohol initiator  
114 pentaerythritol and then methacrylate functionalised. 4PCLMA and pentaerythritol were then added  
115 to a round bottom flask in the presence of toluene stirred using a magnetic stirrer under a nitrogen  
116 atmosphere. The resulting reaction mixture was heated to 130°C, and SnOct<sub>2</sub> was added.  
117 Furthermore, the reaction was stirred continuously for 6 hours at RT prior to solvent removal via rotary  
118 evaporation. For the methacrylation, hydroxyl-terminated PCL was dissolved in DCM, then the  
119 solution was cooled in an ice bath before the addition of TEA (2 molar equivalents). MAAn (2 molar  
120 equivalents) was added dropwise whilst maintaining a low temperature. The reaction was allowed to  
121 stir for 24 hours at RT in the absence of light under nitrogen gas. Finally, the solvent was removed by  
122 rotary evaporation, and the polymer was purified three times by precipitation from methanol at -80°C.

### 123 2.3. Characterisation of 3PCLMA, 4PCL and 4PCLMA

124 Proton (<sup>1</sup>H) nuclear magnetic resonance NMR spectroscopy analysis was performed on an AVANCE III  
125 spectrometer at 400 MHz to confirm the structure of 3PCLMA and 4PCLMA. The spectra were  
126 recorded using an 8.2 kHz acquisition window, with 64 k data points in 16 transients with a 60 s recycle  
127 delay (to ensure full relaxation). Deuterated chloroform was used as a diluent (CDCl<sub>3</sub>). Spectra were  
128 analysed using MestReNova software. Chemical shifts were referenced relative to CDCl<sub>3</sub> at 7.27 ppm.  
129 The degree of methacrylation (DM) of 3PCLMA and 4PCLMA was calculated by comparing the signal  
130 intensity of the methylene groups and the signal intensities of the methacrylate groups from the NMR  
131 data (Equation 1, 2).

$$DM = ((\int \text{methacrylated ends}) / (\int \text{non - methacrylated} + \text{methacrylated ends})) * 100 \quad (1)$$

$$DM = \frac{((\int I_{5.5} + \int I_{6.1}) / 2)}{((\int I_{5.5} + \int I_{6.1}) / 2) + ((\int I_{3.6}) / 2)} * 100 \quad (2)$$

132 Molecular weight and molecular weight distributions of 4PCLMA were determined using a Viscotek  
133 GPCmax VE200 gel permeation chromatography (GPC) system with a differential refractive index  
134 detector (Waters 410). Tetrahydrofuran was used as the eluting solvent at a flow rate of 1 mL/minute  
135 at 40 °C, and polystyrene standards were used as the calibration sample.

## 136 **2.6. Mechanical Characterisation 3PCLMA and 4PCLMA**

137 Dog-bone shaped tensile test samples were fabricated as previously described<sup>23</sup> and mechanical test  
138 was applied as described previously<sup>38</sup>. Briefly, 0.5 mL 4PCLMA and 3PCLMA were pipetted into the  
139 moulds and cured for 3 min on each side. Samples were tested using a uniaxial mechanical testing  
140 machine (BOSE Electroforce Test Instruments, Minnesota, USA) equipped with a 22 N load cell. Grip  
141 distance and extension rate were set to 10 mm and 0.1 mm/s, respectively, and the force and  
142 elongation data were recorded. The stress and strain values were calculated using the cross-sectional  
143 area where force was applied. Young's modulus was determined using the linear-elastic region of each  
144 sample's stress-strain curves. The ultimate tensile strength (UTS) was calculated as that of the  
145 maximum force applied divided by the cross-sectional area of the sample.

## 146 **2.4. Preparation of PolyHIPE Scaffolds**

147 Thiol-PCL PolyHIPEs were manufactured via photopolymerisation with the formulations presented in  
148 Figure 5A. The continuous phase of the emulsion consisted of PCL, thiol, surfactant (Hypermer B246),  
149 and crosslinker were dissolved in the solvent and stirred using an overhead stirrer (Pro40, SciQuip).  
150 The water was added dropwise, and then the emulsion was left to further mix for a further 5 minutes.  
151 Finally, the photoinitiator was added in the absence of light, mixed and transferred to a silicone mould  
152 and cured via Light Hammer<sup>®</sup> 6 UV curing system (Fusion UV Systems Inc, USA) assisted with bench-  
153 top conveyor (LC6E, Fusion UV Systems Inc, USA) with a power output of 200 W/cm<sup>2</sup> at 100% intensity.

154 PCL-Thiol PolyHIPE samples were washed in a Soxhlet extractor for 24 hours with ethanol. For cell  
155 culture, the samples were transferred to a 70% ethanol and distilled water solution for 30 minutes.  
156 The samples were transferred to sterile PBS and washed three times to remove traces of ethanol. To  
157 remove all trapped air from the discs, the samples were kept in a sterile PBS container, a lid affixed  
158 with a 0.2 µm pore syringe filter was used to seal the container, which was then put into a vacuum  
159 oven and cycled from being under vacuum to normal atmospheric pressure to draw the trapped air  
160 out of the sample. This was repeated three times until all the samples remained submerged under  
161 normal atmospheric pressure.

## 162 2.5. Chemical and Morphological Characterisation of PolyHIPEs

163 To prepare the 4PCLMA and 3PCLMA based PolyHIPE specimens for SEM they were first freeze-dried  
164 and cut to reveal their internal cross-section. These were then attached to carbon fibre pads adhered  
165 to aluminium stubs and sputter-coated with gold (Emscope SC500, Philips). The morphologies of the  
166 PolyHIPE disks were then imaged using a Philips XL-20 scanning electron microscope operating at 10.0  
167 kV. The SEM micrographs were analysed using the software Image J 1.48 to quantify the average void  
168 diameter of PolyHIPE disks, the diameters of 90 voids and 20 windows were measured, and a statistical  
169 correction factor was applied to the average void diameter<sup>39</sup>. Pore and window size distribution  
170 histograms were created and average pore (D) and window sizes (d) were reported. The degree of  
171 interconnectivity was calculated by dividing the average window size by the average pore size (d/D)  
172<sup>23,40</sup>, and the degree of openness was calculated by dividing open surface area by total surface area  
173 for randomly selected 10 pores<sup>7,13,17</sup>. Fourier Transform Infrared spectroscopy was performed on  
174 Thiolene 4PCLMA PolyHIPE. Readings were taken between 500 – 4000 cm<sup>-1</sup> and resolution of 4 cm<sup>-1</sup>.

## 175 2.5. Biological Characterisation

### 176 2.5.1. Fibroblast Cell Culture

177 Human dermal fibroblast cells were isolated from tissue samples obtained from consenting patients  
178 undergoing either elective abdominoplasty or breast reduction surgery as described previously<sup>3,23,41</sup>.  
179 The collected tissue was used under the requirements stipulated by the Research Tissue Bank Licence  
180 12179, and fibroblast cells were isolated (Ethical approval for the tissue acquisition was granted by  
181 the local ethical approval committee of the NHS Trust, Sheffield, UK, ethics reference: 15/YH/0177).  
182 The fibroblasts were cultured and expanded in T75 culture flasks until they were ~80% confluent.  
183 Scaffolds were disinfected in ethanol and washed with PBS three times. Dulbecco's modified Eagle's  
184 medium supplemented with 10% FCS, 0.01% L-Glutamine, 0.01% penicillin-streptomycin and 0.0025%  
185 amphotericin B was used as cell culture media. Cells were trypsinised and were seeded with the  
186 concentration of 75000 cells/40 µL media and were left in the incubator at 37°C, 5% CO<sub>2</sub> for 20 minutes  
187 for cell attachment before 1 mL of media was added. The cell medium was changed every three days.

### 188 2.5.2. Bone Cell Culture

189 The manufactured PolyHIPE disks had a diameter of 9 mm, which were washed in acetone and air-  
190 dried prior to the sterilisation process. The PolyHIPE disks were sterilised by immersing in 70% ethanol  
191 for 50 minutes following series of PBS washes (5 minutes, repeated three times). PolyHIPE disks were  
192 then air-dried in a sterilised environment for 48 hours prior to DMEM media soaking for 24 hours.

193 Human osteosarcoma cell line (MG-63) was used to seed disks with the density of 20000 cells (10  $\mu$ L)  
194 per sample and placed in an incubator (37°C and 5% CO<sub>2</sub>) for 30 minutes before addition of 990  $\mu$ L of  
195 cell culture medium and tissue culture plastic was used as control. The samples were left in the  
196 incubator for a period of 3 and 7 days, and the medium was changed every two days.

### 197 2.5.3. Colourimetric Assays

198 Resazurin reduction (RR) assay was applied to measure the cellular metabolic activity and estimate  
199 the cell viability on scaffolds. Resazurin solution (non-fluorescent, blue) is reduced by the cells and  
200 forms resorufin (fluorescent, pink), which is detectable by a fluorescence plate reader. 1 mM resazurin  
201 stock solution in dH<sub>2</sub>O was diluted to 100  $\mu$ M in culture media to make the resazurin working solution.  
202 1 mL of RR solution was added to each well, and the scaffolds were transferred into a fresh well plate  
203 using sterile forceps. The well plates were protected from light and incubated for 4 hours at 37 °C.  
204 From each scaffold, triplicate samples of 200  $\mu$ L of the reduced solution were added to a 96 well plate.  
205 It was measured three times using a spectrofluorometer (FLX800, BIO-TEK Instruments, Inc.) at an  
206 excitation wavelength of 540 nm and an emission wavelength of 630 nm. Scaffolds were washed twice  
207 with PBS before adding fresh media. RR assay was performed at three time points (day 1, day 4, and  
208 day 7) with fresh scaffold/cell constructs for each. The reaction of blank (cell-free) PolyHIPEs with MTT  
209 reagent was also investigated. For this, first, 1 mg/mL MTT solution was prepared in PBS and filter  
210 sterilised. Scaffolds were placed into a fresh 24-well plate, and 1 mL of MTT reagent was added into  
211 each well, covered aluminium foil and incubated for 4 hours and 24 hours at 37°C. Colour change due  
212 to formed formazan crystals was imaged.

### 213 2.5.3. DNA Quantification Assay

214 Quant-iT™ PicoGreen dsDNA Assay kit (Life Technologies, UK) is a DNA quantitation assay used to  
215 determine the cell number. Cell culture medium was removed from samples following series of PBS  
216 washes prior to treatment with 500  $\mu$ L cell assay buffer (1:10 Tris-EDTA (TE) buffer (1.5 M Tris-HCL, 1  
217 mM ZnCl<sub>2</sub>, 1 mM MgCl<sub>2</sub>) in deionised water and 1% Triton-X100) for each time point at room  
218 temperature for 30 minutes following overnight freeze at 4°C. The samples were treated through a  
219 series of freeze-thaw cycles, freeze (-80°C, 10 minutes) and thaw (37°C, 15 minutes) repeated three  
220 times. Following 15 seconds of vortexing and they were centrifuged at 10000 rpm for 5 minutes.  
221 180  $\mu$ L of supernatant was added in 1:1 ratio to PicoGreen reagent (diluted in 1:20 TE buffer (10 mM  
222 Tris-HCL, 1 mM EDTA, pH 7.5), 1:200 PicoGreen in deionised water). The samples were incubated at  
223 room temperature for 10 minutes in darkness prior to fluorescence reading at  $\lambda_{ex}$  = 485 nm and  $\lambda_{em}$  =  
224 528 nm.

## 225 2.5.2. Confocal Microscopy

226 4',6-diamidino-2-phenylindole (DAPI) and TRITC-phalloidin stained specimens were prepared by  
227 diluting the stains (1:1000 in PBS) and incubated at room temperature for 30 minutes in darkness as  
228 described previously<sup>15,17,42</sup>. Single plane images (1024×1024 pixels) were taken via an upright confocal  
229 microscope (Zeiss LSM510-META, UK) assisted with ×10 objective (W-N-Achroplan 10×/N.A. 0.3, Zeiss  
230 ltd, UK). DAPI stain was excited using an 800 nm two-photon Ti-Sapphire laser set to 358 nm  $\lambda_{ex}$ , 461  
231 nm  $\lambda_{em}$ . TRITC and FITC phalloidin (F-actin) was determined via single-photon laser set to  $\lambda_{ex}$  = 495 nm,  
232  $\lambda_{em}$  = 515 nm (FITC) and  $\lambda_{ex}$  = 545 nm,  $\lambda_{em}$  = 573 nm (TRITC).

## 233 2.6. Statistical Analysis

234 Statistical analyses were performed by using GraphPad Prism 6 using one-way and two-way analysis  
235 of variance (ANOVA) for mechanical testing and cellular metabolic activity assays, respectively, and  
236 plotted as mean  $\pm$  SD. A difference was deemed statistically significant if the p-value was less than  
237 0.05, and the statistical differences are denoted in the figures. The total numbers of replicates (n) are  
238 stated in the figure legends.

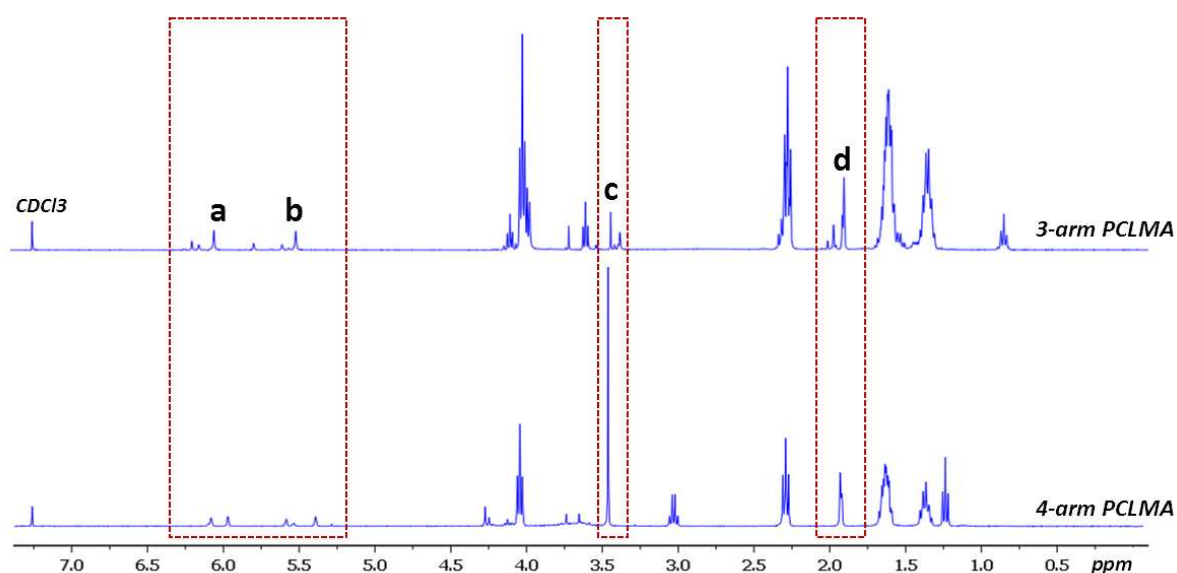
## 239 3. Results and Discussion

### 240 3.1. Synthesis and the characterisation of 3PCLMA and 4PCLMA

241 PCL is one of the most widely used synthetic polymers used to fabricate tissue engineering scaffolds.  
242 Yet, its potential is limited by its form. Typically, PCL is a thermoplastic that is sold as small solid beads  
243 of various high molecular weights (60.000-90.000 g/mol), these can be dissolved in a solvent and  
244 electrospun into a fibrous scaffold, cast into a porous material by porogen leaching, or melted and  
245 extruded into the desired shape<sup>35,43-45</sup>. Photocurable monomers have gained increasing attention  
246 because of their potential to rapidly polymerise (seconds to minutes depending on the sample size)  
247 and their suitability to be used with a variety of fabrication techniques which include 3D printing<sup>4,46,47</sup>,  
248 porogen leaching<sup>48</sup>, and emulsion templating<sup>2,23,24</sup>. There is a limited range of commercially available  
249 degradable monomers. So, *in house* synthesis of photocurable monomers are often used.  
250 Functionalised 2-arm<sup>49-51</sup>, 3-arm<sup>30,52</sup> and 4-arm<sup>2,4,23,24</sup> PCLs are forms of PCL used for tissue  
251 engineering applications. The molecular weight of the polymer<sup>53</sup> it's degree of functionalization<sup>46</sup> and  
252 the number of monomer arms<sup>53</sup> have been shown to influence the mechanical properties of these  
253 polymers. This photo-polymerisation of PCL expands the potential of this material to a range of tissue  
254 engineering applications. The FDA approval of PCL made medical devices on the market is encouraging  
255 for PCL to be used for other biomedical applications<sup>23,54</sup>. With similar motivation, there has been a

256 number of studies in the literature on the development of PCL based PolyHIPE structures either using  
257 radical polymerization or ring-opening polymerization <sup>23,30,55–62</sup>.

258 In this study, the synthesis of 4PCL and methacrylate-functionalisation of both synthesised 4PCL and  
259 commercially available 3PCL is presented. 3PCL and 4PCL were successfully functionalised via  
260 methacrylate functionalisation. According to <sup>1</sup>H NMR analysis (Figure 3), while the non-methacrylated  
261 end of 3PCL and 4PCL has methylene groups adjacent to hydroxyl end groups shown with the peak at  
262 3.6 ppm. On the methacrylated ends, they are converted into methacrylate groups, which are  
263 indicated at peaks 1.9, 5.5 and 6.1 ppm. The degree of methacrylation of 3PCLMA and 4PCLMA was  
264 calculated as 44% and 46%, respectively. The degrees of methacrylation of both 3PCLMA and 4PCLMA  
265 can be controlled using various parameters such as the ratio of methacrylation agents (methacrylic  
266 anhydride and triethylamine) to pre-polymer (PCL) and reaction time of methacrylation. Recently our  
267 group has reported the fabrication route of PCLMA with different degrees of methacrylation and the  
268 effect of methacrylation degree on mechanical properties of PCLMA <sup>63</sup>. In this study, we aimed to keep  
269 the degree of methacrylation constant for both types of polymer to compare their properties. But, the  
270 degree of methacrylation can be increased up to 100% for specific applications, such as bone tissue  
271 engineering scaffolds, as we reported before <sup>4</sup>. In this study, while PCL triol with a molecular weight  
272 of 900 g/mol was used for 3PCLMA, M<sub>w</sub> and M<sub>n</sub> values of 4PCLMA were determined by GPC analysis  
273 as 20900 g/mol and 15000 g/mol, respectively, which gives a dispersity of 1.4.



274  
275 **Figure 3:** Proton NMR spectrum of 3PCLMA and 4PCLMA and the relative assignments. c: the peaks of the  
276 hydroxyl group; a, b, and d are the peaks of the methacrylate group.

277 Mechanical properties of the microenvironment are reported to have a dominant impact on cell  
278 behaviour. It is because cells can sense the stiffness of the material by mechanosensation and directs

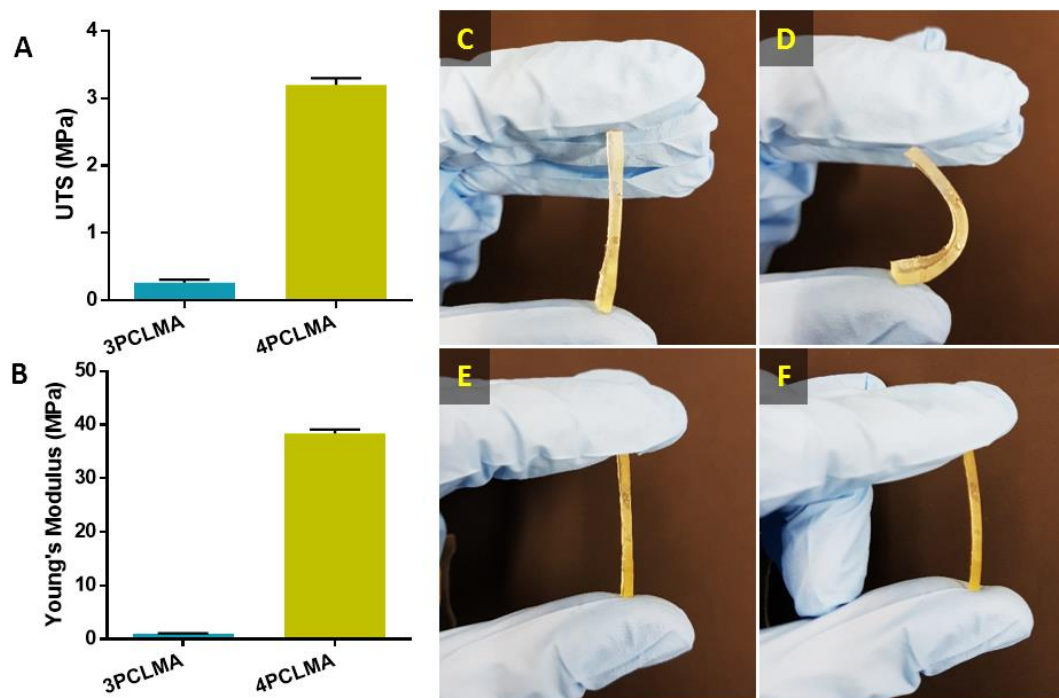
279 its morphology, gene expression, and differentiation, accordingly <sup>64-66</sup>. Accordingly, we have  
280 investigated the mechanical properties of the polymer synthesized in the scope of this study; 3PCLMA  
281 and 4PCLMA. Tensile testing of 3PCLMA and 4PCLMA shows a significant difference between the  
282 mechanical properties of the two polymers. The 4PCLMA had the greater Young's modulus of  
283  $38.37 \pm 0.76$  MPa and UTS of  $3.20 \pm 0.10$  MPa compared to the lower 3PCLMA values of  $1.00 \pm 0.07$  MPa  
284 and  $0.25 \pm 0.04$  MPa (Figure 4A, B). Digital images show the flexibility of 3PCLMA when compressed by  
285 fingers while the more rigid 4PCLMA resisted being bent (Figure 4C-F).

286 Overall; there are two main differences between the structural properties of 3PCLMA and 4PCLMA  
287 used in this study; (i) the number of branching (ii) the molecular weight. The main reasons for these  
288 10-fold and 35-fold differences in UTS and Young's Modulus values of 3PCLMA and 4PCLMA are likely  
289 to be the difference in their crosslinking density and molecular weights (20-folds). 3PCLMA and  
290 4PCLMA have a similar degree of functionalisation, but 4PCLMA has an additional branch, which will  
291 increase the crosslinking. Green et al. reported the UTS and tensile modulus of 79% acrylate-  
292 functionalised 3PCL (3PCLA, Mw: 900 g/mol) as  $0.58 \pm 0.05$  MPa and  $4.0 \pm 0.5$  MPa, respectively. This is  
293 also in line with the value reported by Field et al. of  $3.51 \pm 0.5$  MPa for 77% methacrylate functionalized  
294 3PCL (3PCLMA, Mw 900 g/mol) <sup>63</sup>. Around 2 to the 4-fold difference between these mechanical  
295 properties is likely to be the difference in the degree of functionalisation.

296 It has been reported that an increasing number of arms enhance the mechanical properties of  
297 polymers <sup>53,67</sup>. Doganci et al. also, previously reported that three-armed star-shaped PCL has  
298 significantly lower elastic modulus due to high molecular chain mobility of 3-arm PCL compared to  
299 linear, four- and six-armed PCLs <sup>68</sup>.

300 Secondly, an increase in the higher molecular weight of the polymers generally increases the  
301 mechanical strength of polymers and the glass transition temperature which has an impact on the  
302 storage modulus <sup>69</sup>. Tian et al. investigated the effects of molecular weight on properties of PCL  
303 networks and revealed that the length of the molecular chains directly influences the thermal and  
304 mechanical properties of the networks. Melting temperature ( $T_m$ ), crystallinity, the crystallization  
305 temperature of the prepared PCL networks was shown to increase with increasing molecular weight.  
306 Also, polymers with higher molecular weight resulted in enhanced mechanical strength which was  
307 attributed to a higher degree of crystallization <sup>70,71</sup>. Similarly, Wang et al. reported the role of  
308 crystallinity on mechanical properties of photo-crosslinked poly(3-caprolactone fumarate)  
309 networks <sup>72</sup>.

310



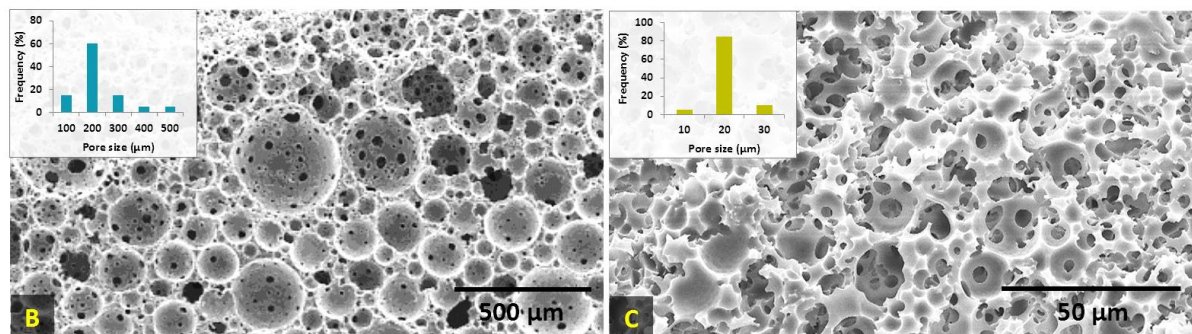
311  
 312 **Figure 4:** (A) UTS, and (B) Young's Modulus values obtained from tensile testing of 3PCLMA and 4PCLMA  
 313 (mean  $\pm$  STD error bars,  $n = 3$ ). Digital photographs highlight the elastic properties of (C, D) 3PCLMA and (E, F)  
 314 4PCLMA before and during finger compression, respectively.

### 315 3.2. Fabrication of PCLMA PolyHIPE Scaffolds

316 The emulsion ingredients and SEM pictures of the corresponding Thiol-3PCLMA and Thiol-4PCLMA  
 317 PolyHIPEs are given in Figure 5A. The impact of solvent type and amount<sup>23</sup>, water volume<sup>17</sup>, emulsion  
 318 temperature<sup>73</sup>, and surfactant composition<sup>74</sup> on the morphology of the emulsion templated scaffolds  
 319 has been previously reported. We intended to produce scaffolds with different pore sizes ranging from  
 320 ten to a few hundred micrometres to show the tunability of this manufacturing method. Average pore  
 321 sizes of thiol-3PCLMA PolyHIPE and thiol-4PCLMA PolyHIPE were calculated as  $176.4 \pm 82.2 \mu\text{m}$  and  
 322  $15.7 \pm 3.0 \mu\text{m}$ , respectively (Figure 5). Both of the formulations of PolyHIPE have shown open cellular  
 323 morphology which is characterised by the presence of the windows between neighbouring pores  
 324 (Figure 5B, C). The average window sizes were measured as  $7.8 \pm 8.9 \mu\text{m}$  and  $4.5 \pm 1.7 \mu\text{m}$  for the same  
 325 groups, respectively. DOI and DOO values of thiol-4PCLMA PolyHIPE samples were calculated 7 and  
 326 3.6 fold higher than DOI and DOO values of thiol-3PCLMA PolyHIPEs. Although the number of pores  
 327 was significantly higher in thiol-3PCLMA PolyHIPEs, as their relative window diameter (to the pore  
 328 size) is smaller, it resulted in lower DOI and DOO in thiol-3PCLMA PolyHIPEs compared to thiol-  
 329 4PCLMA PolyHIPE.

330

Group	PCL (g)	Trithiol (g)	Surf. (g)	Crosslinker (g)	Solvent (g)	PI (g)	H <sub>2</sub> O (mL)	T (°C)	D <sup>a</sup> (μm)	d <sup>b</sup> (μm)	DOI <sup>c</sup>	DOO <sup>d</sup>	Porosity <sup>e</sup>	Density <sup>f</sup> (g/cm <sup>3</sup> )
3PCLMA	0.17	0.18	0.15	0.11 (TMPTA)	0.27 (CHCl <sub>3</sub> )	0.03	4	60	176.4 ± 82.2	7.8 ± 8.9	0.04	0.07	87	0.14
4PCLMA	5.00	3.22	0.15	2.50 (TMPTMA)	11.25 (DCE)	0.56	35	23	15.7 ± 3.0	4.5 ± 1.7	0.28	0.25	77	0.26



331

332 **Figure 5:** (A) Composition, (B, C) Pore size distribution histograms and SEM micrographs of thiol-3PCLMA  
 333 PolyHIPE and thiol-4PCLMA PolyHIPE, respectively. (a: average pore size, b: average window size, c: degree of  
 334 interconnectivity, d: degree of openness, e: nominal porosity, f: expected density calculated based on porosity).

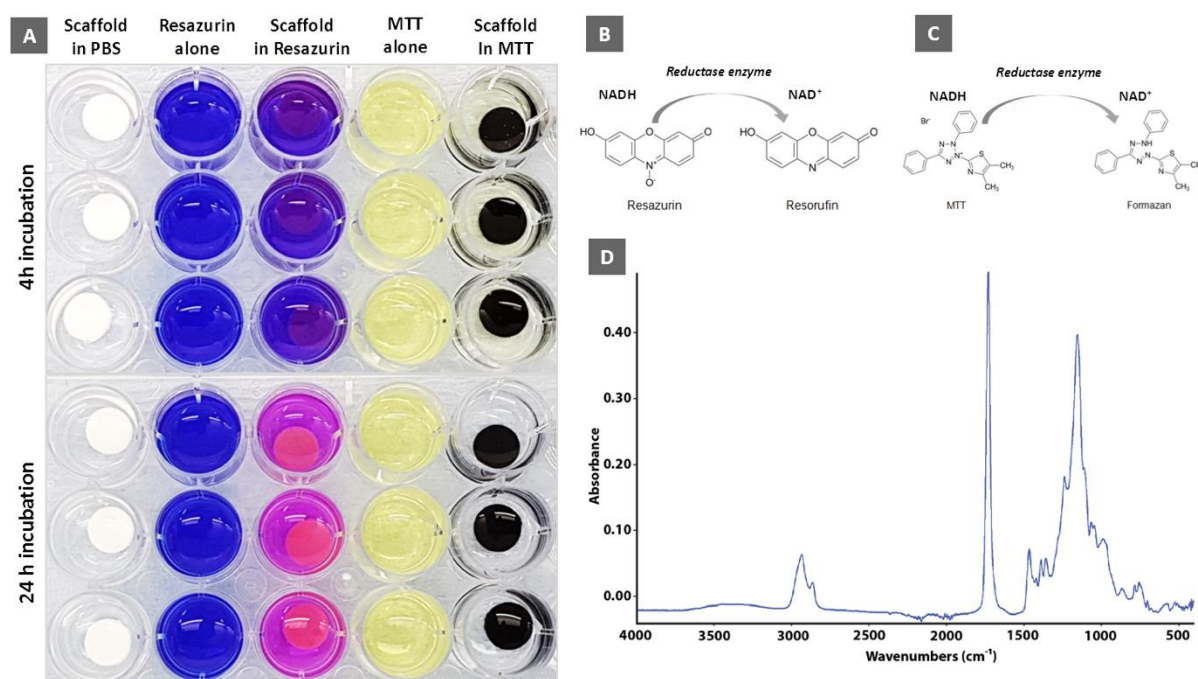
335 As higher temperature also reduced the emulsion stability, the pore size distribution of 3PCLMA based  
 336 PolyHIPE compared to the 4PCLMA was comparably wider (Figure 5B, C), which results in a significantly  
 337 higher standard deviation than the average pore size seen in PolyHIPE scaffolds<sup>26,40</sup>. It is likely that  
 338 the higher emulsion mixing temperature of 60°C is the main factor for the difference in the pore size  
 339 between these samples as this reduces the emulsion stability, which causes more droplet coalescence  
 340 and therefore larger pores. Also, there was a significant difference between the forms and viscosities  
 341 of the polymers used in this study; while 3PCLMA was runny, liquid, 4PCLMA was solid at room  
 342 temperature. This can be explained with ~20-folds molecular weight difference between 3PCLMA and  
 343 4PCLMA, as the viscosity of PCL is expected to increase with increasing molecular weight<sup>45,75</sup>. As the  
 344 viscosity of the polymer directly affects the mixing efficiency of the two phases and emulsion  
 345 formation, this may also contribute to a significant morphological difference between PolyHIPE  
 346 groups. Additionally, the type of the diluting solvent used in the composition was reported to have  
 347 an impact on the emulsion stability and average pore size of PolyHIPEs<sup>23</sup>. As chloroform has a higher  
 348 density (1.480 g/mL) than DCE (1.256 g/mL), its use as a diluting solvent in the oil phase increases the  
 349 density difference between the oil and water phase which increases the velocity of a single droplet in  
 350 the emulsion according to Stoke`s Equation<sup>7</sup> and results in larger pore size.

### 351 3.3. Biological characterisation of PolyHIPE scaffolds

352 To assess the biocompatibility of the scaffolds, initially, an MTT assay was used. However, it was found  
 353 that the scaffold alone also gave a positive signal from MTT (Figure 6). Also, Resazurin Reduction Assay

354 without any cells gave a false-positive result (Figure 6). MTT and RR assays are based on reduction of  
 355 resazurin and MTT by reductase enzyme, present in mitochondria of metabolically active cells, into  
 356 resorufin and formazan crystals, respectively. The initial blue and yellow colours are expected to turn  
 357 to pink and black for MTT and RR, respectively.

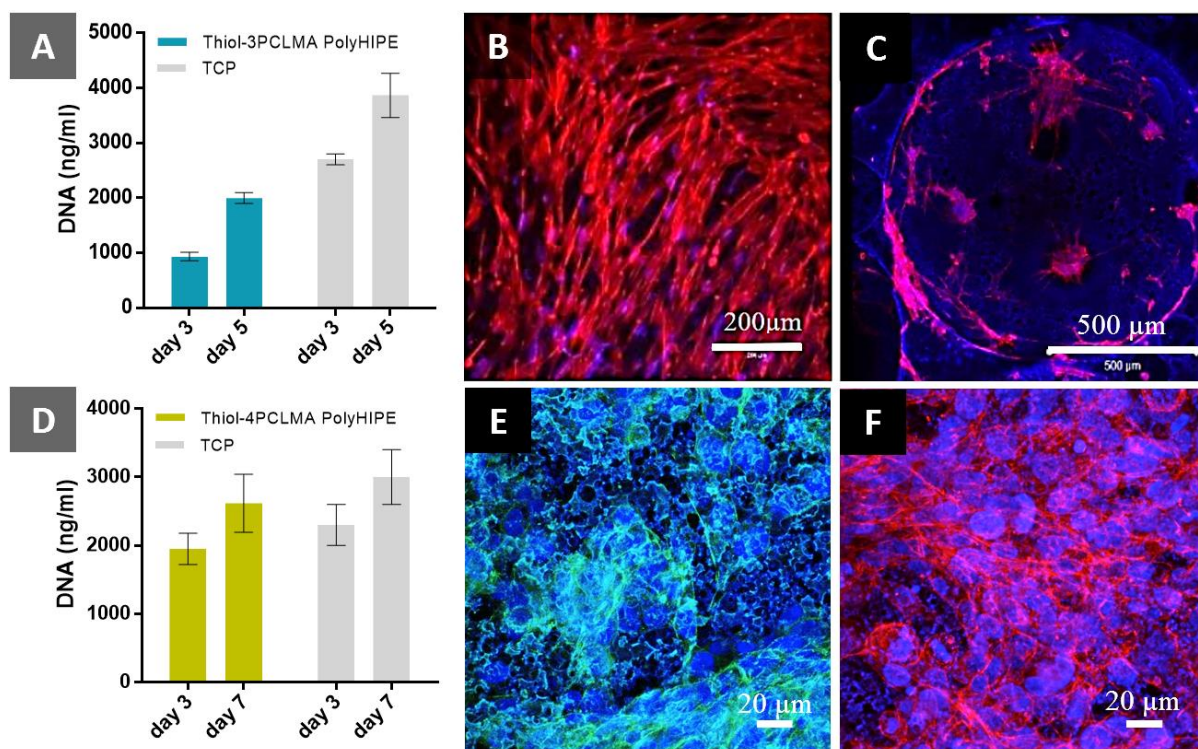
358 FTIR spectrometry of the scaffolds shown free -SH groups on the polymer, which are likely the reducing  
 359 agents for the metabolic dyes (small band between 685-690  $\text{cm}^{-1}$  representing S-H band). So, the  
 360 correlation of cell growth using their metabolic activity via MTT and RR is likely to provide spurious  
 361 false-positive results. The fluorescence of the blanks samples should be measured and subtracted as  
 362 a background absorbance to avoid overestimation of cell viability due to this noise <sup>76</sup>. Similarly,  
 363 Langford et al. have shown the residual thiols of thiolene (meth)acrylate PolyHIPEs using Ellman's  
 364 assay, which is a colourimetric assay <sup>33</sup>.



365  
 366 **Figure 6:** (A) Testing the reaction of the scaffold (without any cells) itself with resazurin and MTT solutions. C/PBS:  
 367 scaffold in PBS (control of scaffold), C/RR: resazurin solution alone (control of resazurin solution (RS)), S/RR:  
 368 scaffold in RS (to test the reaction of the scaffold with RS), C/MTT: MTT solution alone (control of MTT solution),  
 369 S/MTT: scaffold in MTT solution (to test the reaction of the scaffold with MTT solution), Incubation PCL Thiol  
 370 PolyHIPE Discs in Resazurin Reduction and MTT solution. Working principles of (B) Resazurin Reduction assay and  
 371 (C) MTT assay. (D) FTIR spectrum of PolyHIPE disks.

372 In order to overcome the problem associated with MTT and RR assays being reduced by the polymer,  
 373 PicoGreen DNA quantification assay was used to assess the DNA content of the samples to determine  
 374 the biocompatibility of PolyHIPE scaffolds. According to PicoGreen data, the cell viability of fibroblasts

375 shown an increasing trend from day three to day five on thiol-PCLMA PolyHIPEs (Figure 7A). A confocal  
 376 image of seven days culture of fibroblast on flat sheets of thiol-3PCLMA polymer (not PolyHIPE) shows  
 377 that cells attached, proliferated, and elongated on the polymer surface. Similarly, fibroblasts sit on the  
 378 pores and spread over the walls of the PolyHIPE scaffold. Although polymer gives a blue background,  
 379 Phalloiding TRITC staining clearly shown the cell cytoskeleton. Blue autofluorescence of thiol-PCL  
 380 based PolyHIPEs also has been reported <sup>30</sup>. Similarly, the cell viability of MG63s on Thiol-4PCLMA  
 381 PolyHIPE showed an increasing trend from day 3 to day 7. Seven days culture of MG63s were stained  
 382 with both Phalloidin FITC and Phalloidin TRITC. Confocal images of both stainings show that cells  
 383 elongated and spread over the pores of the PolyHIPE scaffold.



384  
 385 **Figure 7:** (A) Cell viability of fibroblasts on thiol-3PCLMA PolyHIPE scaffolds (n=3). (B) Confocal image of 7-days  
 386 culture of fibroblasts growing on thiol-3PCLMA. (C) Fluorescent confocal images of human dermal fibroblast cells  
 387 growing on the PCL/Thiol PolyHIPE. (D) Cell viability of MG36s on thiol-4PCLMA PolyHIPE scaffolds (n=3). (E-F)  
 388 Confocal image of 7-days culture of MG63s growing on thiol-4PCLMA. DAPI: blue, Phalloidin FITC: green, and  
 389 Phalloidin TRITC: red.

390 Previously Johnson et al. also reported the cell viability of L929 fibroblast on thiol-triacrylate  
 391 functionalised PCL PolyHIPEs <sup>30</sup>. In this study, similar to our previous finding, cells tend to locate in the  
 392 pores of PolyHIPEs with pore size larger than 20  $\mu\text{m}$ , while they spread over the pores that have a  
 393 diameter less than 20  $\mu\text{m}$  <sup>23</sup>. Both 3PCLMA and 4PCLMA based thiolene PolyHIPEs have been shown  
 394 to support cell attachment and cell viability.

#### 395 **4. Conclusion**

396 In this study, thiol based PolyHIPEs using either 3PCLMA or 4PCLMA were fabricated successfully, and  
397 a tunability porosity was demonstrated. *In vitro* biocompatibility of PolyHIPEs was investigated using  
398 both HDFs and MG63 cells, and thiolene/acrylate-based PolyHIPEs were shown to provide a  
399 biocompatible substrate in terms of cell attachment and viability. In conclusion, this research  
400 demonstrated a route to synthesise novel Poly-HIPE PCL-based biomaterial that could be suitable for  
401 tissue engineering and regenerative medicine applications.

#### 402 **5. Acknowledgements**

403 The authors gratefully acknowledge the Republic of Turkey – The Ministry of National Education for  
404 funding Betül Aldemir Dikici and Serkan Dikici. We acknowledge the Engineering and Physical Sciences  
405 Research Council (Grant No. EP/I007695/1) and the Medical Research Council (Grant No.  
406 MR/L012669/1) for funding the equipment used in this study. We are grateful to the UK Engineering  
407 and Physical Sciences Research Council (EPSRC) for supporting this work with a PhD studentship of AM  
408 with the “White Rose” DTC in Tissue Engineering & Regenerative Medicine (EP/L014823/1) and to The  
409 EPSRC Centre for Innovative Manufacturing in Medical Devices (MeDe Innovation, grant number  
410 EP/K029592/1). NC thanks to the Australian Research Council for support (DP190103309). We thank  
411 Dr Sandra van Meurs for her help on NMR analysis, interpretation, and calculation of the degree of  
412 functionalisation.

#### 413 **6. Author contributions**

414 BAD contributed to the experimental design, analysis, data acquisition, and interpretation of data,  
415 statistical analysis, and drafting of the manuscript. AM contributed to the experimental design,  
416 analysis, data acquisition, interpretation of data and drafting of the manuscript. CS, SD, TP, and LD  
417 contributed to the experimental design, analysis, and data acquisition. CL and NC provided technical  
418 knowledge and equipment training. PH, IO, SM, NC, and FC contributed with their supervision and  
419 critical revision and editing of the manuscript.

#### 420 **References**

- 421 (1) Mangir, N.; Aldemir Dikici, B.; Chapple, C. R.; MacNeil, S. Landmarks in Vaginal Mesh Development:  
422 Polypropylene Mesh for Treatment of SUI and POP. *Nat. Rev. Urol.* **2019**, *16* (11), 675–689.  
423 <https://doi.org/10.1038/s41585-019-0230-2>.
- 424 (2) Dikici, S.; Aldemir Dikici, B.; Bhaloo, S. I.; Balcells, M.; Edelman, E. R.; MacNeil, S.; Reilly, G. C.; Sherborne,  
425 C.; Claeysens, F. Assessment of the Angiogenic Potential of 2-Deoxy-D-Ribose Using a Novel in Vitro 3D  
426 Dynamic Model in Comparison With Established in Vitro Assays. *Front. Bioeng. Biotechnol.* **2020**, *7* (451),

- 427 1–20. <https://doi.org/10.3389/fbioe.2019.00451>.
- 428 (3) Dikici, S.; Claeysens, F.; MacNeil, S. Bioengineering Vascular Networks to Study Angiogenesis and  
429 Vascularization of Physiologically Relevant Tissue Models in Vitro. *ACS Biomater. Sci. Eng.* **2020**, *6* (6),  
430 3513–3528. <https://doi.org/10.1021/acsbiomaterials.0c00191>.
- 431 (4) Aldemir Dikici, B.; Reilly, G. C.; Claeysens, F. Boosting the Osteogenic and Angiogenic Performance of  
432 Multiscale Porous Polycaprolactone Scaffolds by in Vitro Generated Extracellular Matrix Decoration. *ACS*  
433 *Appl. Mater. Interfaces* **2020**, *12* (11), 12510–12524. <https://doi.org/10.1021/acsaami.9b23100>.
- 434 (5) Thadavirul, N.; Pavasant, P.; Supaphol, P. Development of Polycaprolactone Porous Scaffolds by  
435 Combining Solvent Casting, Particulate Leaching, and Polymer Leaching Techniques for Bone Tissue  
436 Engineering. *J. Biomed. Mater. Res. Part A* **2014**, *102* (10), 3379–3392.  
437 <https://doi.org/10.1002/jbm.a.35010>.
- 438 (6) Owen, R.; Sherborne, C.; Evans, R.; C. Reilly, G.; Claeysens, F. Combined Porogen Leaching and Emulsion  
439 Templating to Produce Bone Tissue Engineering Scaffolds. *Int. J. Bioprinting* **2020**, *6* (2), 99–113.  
440 <https://doi.org/10.18063/ijb.v6i2.265>.
- 441 (7) Aldemir Dikici, B.; Claeysens, F. Basic Principles of Emulsion Templating and Its Use as an Emerging  
442 Manufacturing Method of Tissue Engineering Scaffolds. *Front. Bioeng. Biotechnol.* **2020**, *8* (875), 1–32.  
443 <https://doi.org/10.3389/fbioe.2020.00875>.
- 444 (8) Cameron, N. R. High Internal Phase Emulsion Templating as a Route to Well-Defined Porous Polymers.  
445 *Polymer (Guildf)*. **2005**, *46* (5), 1439–1449. <https://doi.org/10.1016/j.polymer.2004.11.097>.
- 446 (9) Silverstein, M. S. PolyHIPEs: Recent Advances in Emulsion-Templated Porous Polymers. *Prog. Polym. Sci.*  
447 **2014**, *39* (1), 199–234. <https://doi.org/10.1016/j.progpolymsci.2013.07.003>.
- 448 (10) Silverstein, M. S. Emulsion-Templated Porous Polymers: A Retrospective Perspective. *Polymer (Guildf)*.  
449 **2014**, *55* (1), 304–320. <https://doi.org/10.1016/j.polymer.2013.08.068>.
- 450 (11) Zhang, T.; Sanguramath, R. A.; Israel, S.; Silverstein, M. S. Emulsion Templating: Porous Polymers and  
451 Beyond. *Macromolecules* **2019**, *52* (15), 5445–5479. <https://doi.org/10.1021/acs.macromol.8b02576>.
- 452 (12) Silverstein, M. S.; Cameron, N. R. PolyHIPEs - Porous Polymers from High Internal Phase Emulsions. In  
453 *Encyclopedia of Polymer Science and Technology*; 2010. <https://doi.org/10.1002/0471440264.pst571>.
- 454 (13) Pulko, I.; Krajnc, P. High Internal Phase Emulsion Templating - A Path to Hierarchically Porous Functional  
455 Polymers. *Macromol. Rapid Commun.* **2012**, *33* (20), 1731–1746.  
456 <https://doi.org/10.1002/marc.201200393>.
- 457 (14) Kramer, S.; Cameron, N. R.; Krajnc, P. Porous Polymers from High Internal Phase Emulsions as Scaffolds  
458 for Biological Applications. *Polymers (Basel)*. **2021**, *13* (11), 1786.  
459 <https://doi.org/10.3390/polym13111786>.
- 460 (15) Malayeri, A.; Sherborne, C.; Paterson, T.; Mittar, S.; Asencio, I. O.; Hatton, P. V.; Claeysens, F.  
461 Osteosarcoma Growth on Trabecular Bone Mimicking Structures Manufactured via Laser Direct Write.  
462 *Int. J. Bioprinting* **2016**, *2* (2), 67–77. <https://doi.org/10.18063/IJB.2016.02.005>.
- 463 (16) Johnson, D. W.; Sherborne, C.; Didsbury, M. P.; Pateman, C.; Cameron, N. R.; Claeysens, F.  
464 Macrostructuring of Emulsion-Templated Porous Polymers by 3D Laser Patterning. *Adv. Mater.* **2013**, *25*  
465 (23), 3178–3181. <https://doi.org/10.1002/adma.201300552>.
- 466 (17) Owen, R.; Sherborne, C.; Reilly, G. C.; Claeysens, F.; Paterson, T.; Green, N. H.; Reilly, G. C.; Claeysens,  
467 F. Emulsion Templated Scaffolds with Tunable Mechanical Properties for Bone Tissue Engineering. *J.*

- 468 *Mech. Behav. Biomed. Mater.* **2016**, *54* (2016), 159–172. <https://doi.org/10.1016/j.jmbbm.2015.09.019>.
- 469 (18) Gitli, T.; Silverstein, M. S. Bicontinuous Hydrogel–Hydrophobic Polymer Systems Through Emulsion  
470 Templated Simultaneous Polymerizations. *Soft Matter* **2008**, *4* (12), 2475.  
471 <https://doi.org/10.1039/b809346f>.
- 472 (19) Lépine, O.; Birot, M.; Deleuze, H. Preparation of a Poly(Furfuryl Alcohol)-Coated Highly Porous  
473 Polystyrene Matrix. *Macromol. Mater. Eng.* **2009**, *294* (9), 599–604.  
474 <https://doi.org/10.1002/mame.200900102>.
- 475 (20) Akay, G.; Birch, M. A.; Bokhari, M. A. Microcellular PolyHIPE Polymer Supports Osteoblast Growth and  
476 Bone Formation in Vitro. *Biomaterials* **2004**, *25* (18), 3991–4000.  
477 <https://doi.org/10.1016/j.biomaterials.2003.10.086>.
- 478 (21) Naranda, J.; Sušec, M.; Maver, U.; Gradišnik, L.; Gorenjak, M.; Vukasović, A.; Ivković, A.; Rupnik, M. S.;  
479 Vogrin, M.; Krajnc, P. Polyester Type PolyHIPE Scaffolds with an Interconnected Porous Structure for  
480 Cartilage Regeneration. *Sci. Rep.* **2016**, *6* (1), 28695. <https://doi.org/10.1038/srep28695>.
- 481 (22) Huš, S.; Krajnc, P. PolyHIPEs from Methyl Methacrylate: Hierarchically Structured Microcellular Polymers  
482 with Exceptional Mechanical Properties. *Polymer (Guildf)*. **2014**, *55* (17), 4420–4424.  
483 <https://doi.org/10.1016/j.polymer.2014.07.007>.
- 484 (23) Aldemir Dikici, B.; Sherborne, C.; Reilly, G. C.; Claeysens, F. Emulsion Templated Scaffolds Manufactured  
485 from Photocurable Polycaprolactone. *Polymer (Guildf)*. **2019**, *175* (2019), 243–254.  
486 <https://doi.org/10.1016/j.polymer.2019.05.023>.
- 487 (24) Aldemir Dikici, B.; Dikici, S.; Reilly, G. C.; MacNeil, S.; Claeysens, F. A Novel Bilayer Polycaprolactone  
488 Membrane for Guided Bone Regeneration: Combining Electrospinning and Emulsion Templating.  
489 *Materials (Basel)*. **2019**, *12* (16), 2643. <https://doi.org/10.3390/ma12162643>.
- 490 (25) Wang, A.; Paterson, T.; Owen, R.; Sherborne, C.; Dugan, J.; Li, J.; Claeysens, F. Photocurable High Internal  
491 Phase Emulsions (HIPEs) Containing Hydroxyapatite for Additive Manufacture of Tissue Engineering  
492 Scaffolds with Multi-Scale Porosity. *Mater. Sci. Eng. C* **2016**, *67* (2016), 51–58.  
493 <https://doi.org/10.1016/j.msec.2016.04.087>.
- 494 (26) Caldwell, S.; Johnson, D. W.; Didsbury, M. P.; Murray, B. A.; Wu, J. J.; Przyborski, S. A.; Cameron, N. R.  
495 Degradable Emulsion-Templated Scaffolds for Tissue Engineering from Thiol-Ene Photopolymerisation.  
496 *Soft Matter* **2012**, *8* (40), 10344–10351. <https://doi.org/10.1039/c2sm26250a>.
- 497 (27) Kimmins, S. D.; Wyman, P.; Cameron, N. R. Photopolymerised Methacrylate-Based Emulsion-Templated  
498 Porous Polymers. *React. Funct. Polym.* **2012**, *72* (12), 947–954.  
499 <https://doi.org/10.1016/j.reactfunctpolym.2012.06.015>.
- 500 (28) Sears, N. A.; Dhavalikar, P. S.; Cosgriff-Hernandez, E. M. Emulsion Inks for 3D Printing of High Porosity  
501 Materials. *Macromol. Rapid Commun.* **2016**, *37* (16), 1369–1374.  
502 <https://doi.org/10.1002/marc.201600236>.
- 503 (29) Lovelady, E.; Kimmins, S. D.; Wu, J.; Cameron, N. R. Preparation of Emulsion-Templated Porous Polymers  
504 Using Thiol-Ene and Thiol-Yne Chemistry. *Polym. Chem.* **2011**, *2* (3), 559–562.  
505 <https://doi.org/10.1039/c0py00374c>.
- 506 (30) Johnson, D. W.; Langford, C. R.; Didsbury, M. P.; Lipp, B.; Przyborski, S. A.; Cameron, N. R. Fully  
507 Biodegradable and Biocompatible Emulsion Templated Polymer Scaffolds by Thiol-Acrylate  
508 Polymerization of Polycaprolactone Macromonomers. *Polym. Chem.* **2015**, *6* (41), 7256–7263.  
509 <https://doi.org/10.1039/c5py00721f>.

- 510 (31) Sušec, M.; Liska, R.; Russmüller, G.; Kotek, J.; Krajnc, P. Microcellular Open Porous Monoliths for Cell  
511 Growth by Thiol-Ene Polymerization of Low-Toxicity Monomers in High Internal Phase Emulsions.  
512 *Macromol. Biosci.* **2015**, *15* (2), 253–261. <https://doi.org/10.1002/mabi.201400219>.
- 513 (32) Whitely, M. E.; Robinson, J. L.; Stuebben, M. C.; Pearce, H. A.; McEnery, M. A. P.; Cosgriff-Hernandez, E.  
514 Prevention of Oxygen Inhibition of PolyHIPE Radical Polymerization Using a Thiol-Based Cross-Linker.  
515 *ACS Biomater. Sci. Eng.* **2017**, *3* (3), 409–419. <https://doi.org/10.1021/acsbiomaterials.6b00663>.
- 516 (33) Langford, C. R.; Johnson, D. W.; Cameron, N. R. Chemical Functionalization of Emulsion-Templated  
517 Porous Polymers by Thiol-Ene “Click” Chemistry. *Polym. Chem.* **2014**, *5* (21), 6200–6206.  
518 <https://doi.org/10.1039/c4py00713a>.
- 519 (34) da Silva, M. A.; Crawford, A.; Mundy, J.; Martins, A.; Araújo, J. V.; Hatton, P. V.; Reis, R. L.; Neves, N. M.  
520 Evaluation of Extracellular Matrix Formation in Polycaprolactone and Starch-Compounded  
521 Polycaprolactone Nanofiber Meshes When Seeded with Bovine Articular Chondrocytes. *Tissue Eng. Part*  
522 *A* **2009**, *15* (2), 377–385. <https://doi.org/10.1089/ten.tea.2007.0327>.
- 523 (35) Dikici, S.; Claeysens, F.; MacNeil, S. Pre-Seeding of Simple Electrospun Scaffolds with a Combination of  
524 Endothelial Cells and Fibroblasts Strongly Promotes Angiogenesis. *Tissue Eng. Regen. Med.* **2020**, *17* (4),  
525 445–458. <https://doi.org/10.1007/s13770-020-00263-7>.
- 526 (36) Dikici, S.; Aldemir Dikici, B.; MacNeil, S.; Claeysens, F. Decellularised Extracellular Matrix Decorated PCL  
527 PolyHIPE Scaffolds for Enhanced Cellular Activity, Integration and Angiogenesis. *Biomater. Sci.* **2021**, Just  
528 accepted. <https://doi.org/10.1039/D1BM01262B>.
- 529 (37) Aldemir Dikici, B. Development of Emulsion Templated Matrices and Their Use in Tissue Engineering  
530 Applications, The University of Sheffield, 2020.
- 531 (38) Dikici, S.; Mangır, N.; Claeysens, F.; Yar, M.; MacNeil, S. Exploration of 2-Deoxy-D-Ribose and 17β-  
532 Estradiol as Alternatives to Exogenous VEGF to Promote Angiogenesis in Tissue-Engineered Constructs.  
533 *Regen. Med.* **2019**, *14* (3), 179–197. <https://doi.org/10.2217/rme-2018-0068>.
- 534 (39) Carnachan, R. J.; Bokhari, M.; Przyborski, S. A.; Cameron, N. R. Tailoring the Morphology of Emulsion-  
535 Templated Porous Polymers. *Soft Matter* **2006**, *2* (7), 608. <https://doi.org/10.1039/b603211g>.
- 536 (40) Huš, S.; Kolar, M.; Krajnc, P. Tailoring Morphological Features of Cross-Linked Emulsion-Templated  
537 Poly(Glycidyl Methacrylate). *Des. Monomers Polym.* **2015**, *18* (7), 698–703.  
538 <https://doi.org/10.1080/15685551.2015.1070503>.
- 539 (41) Dikici, S.; Claeysens, F.; MacNeil, S. Decellularised Baby Spinach Leaves and Their Potential Use in Tissue  
540 Engineering Applications: Studying and Promoting Neovascularisation. *J. Biomater. Appl.* **2019**, *0* (0), 1–  
541 14. <https://doi.org/10.1177/0885328219863115>.
- 542 (42) Dikici, S.; Bullock, A. J.; Yar, M.; Claeysens, F.; MacNeil, S. 2-Deoxy-d-Ribose (2dDR) Upregulates Vascular  
543 Endothelial Growth Factor (VEGF) and Stimulates Angiogenesis. *Microvasc. Res.* **2020**, *131*, 104035.  
544 <https://doi.org/10.1016/j.mvr.2020.104035>.
- 545 (43) Bak, T. Y.; Kook, M. S.; Jung, S. C.; Kim, B. H. Biological Effect of Gas Plasma Treatment on CO<sub>2</sub> Gas  
546 Foaming/Salt Leaching Fabricated Porous Polycaprolactone Scaffolds in Bone Tissue Engineering. *J.*  
547 *Nanomater.* **2014**, *2014*, 1–6. <https://doi.org/10.1155/2014/657542>.
- 548 (44) Reignier, J.; Huneault, M. A. Preparation of Interconnected Poly(E[lunate]-Caprolactone) Porous  
549 Scaffolds by a Combination of Polymer and Salt Particulate Leaching. *Polymer (Guildf).* **2006**, *47* (13),  
550 4703–4717. <https://doi.org/10.1016/j.polymer.2006.04.029>.
- 551 (45) Elomaa, L.; Teixeira, S.; Hakala, R.; Korhonen, H.; Grijpma, D. W.; Seppälä, J. V. Preparation of Poly(ε-

- 552 Caprolactone)-Based Tissue Engineering Scaffolds by Stereolithography. *Acta Biomater.* **2011**, 7 (11),  
553 3850–3856. <https://doi.org/10.1016/j.actbio.2011.06.039>.
- 554 (46) Singh, D.; Harding, A. J.; Albadawi, E.; Boissonade, F. M.; Haycock, J. W.; Claeysens, F. Additive  
555 Manufactured Biodegradable Poly(Glycerol Sebacate Methacrylate) Nerve Guidance Conduits. *Acta*  
556 *Biomater.* **2018**, 78 (2018), 48–63. <https://doi.org/10.1016/j.actbio.2018.07.055>.
- 557 (47) Pashneh-Tala, S.; Owen, R.; Bahmaee, H.; Rekštytė, S.; Malinauskas, M.; Claeysens, F. Synthesis,  
558 Characterization and 3D Micro-Structuring via 2-Photon Polymerization of Poly(Glycerol Sebacate)-  
559 Methacrylate—An Elastomeric Degradable Polymer. *Front. Phys.* **2018**, 6 (41), 1–17.  
560 <https://doi.org/10.3389/fphy.2018.00041>.
- 561 (48) Pashneh-Tala, S.; Moorehead, R.; Claeysens, F. Hybrid Manufacturing Strategies for Tissue Engineering  
562 Scaffolds Using Methacrylate Functionalised Poly(Glycerol Sebacate). *J. Biomater. Appl.* **2020**, 34 (8),  
563 1114–1130. <https://doi.org/10.1177/0885328219898385>.
- 564 (49) Busby, W.; Cameron, N. R.; Jahoda, C. A. B. Tissue Engineering Matrixes by Emulsion Templating. *Polym.*  
565 *Int.* **2002**, 51 (10), 871–881. <https://doi.org/10.1002/pi.934>.
- 566 (50) Busby, W.; Cameron, N. R.; Jahoda, C. A. B. Emulsion-Derived Foams (PolyHIPEs) Containing Poly(Se-  
567 Caprolactone) as Matrixes for Tissue Engineering. *Biomacromolecules* **2001**, 2 (1), 154–164.  
568 <https://doi.org/10.1021/bm0000889>.
- 569 (51) Moglia, R. S.; Robinson, J. L.; Muschenborn, A. D.; Touchet, T. J.; Maitland, D. J.; Cosgriff-Hernandez, E.  
570 Injectable PolyMIPE Scaffolds for Soft Tissue Regeneration. *Polymer (Guildf)*. **2014**, 55 (1), 426–434.  
571 <https://doi.org/10.1016/j.polymer.2013.09.009>.
- 572 (52) Diez-Ahedo, R.; Mendibil, X.; Márquez-Posadas, M. C.; Quintana, I.; González, F.; Rodríguez, F. J.; Zilic, L.;  
573 Sherborne, C.; Glen, A.; Taylor, C. S.; et al. UV-Casting on Methacrylated PCL for the Production of a  
574 Peripheral Nerve Implant Containing an Array of Porous Aligned Microchannels. *Polymers (Basel)*. **2020**,  
575 12 (4), 971. <https://doi.org/10.3390/polym12040971>.
- 576 (53) Green, B. J.; Worthington, K. S.; Thompson, J. R.; Bunn, S. J.; Rethwisch, M.; Kaalberg, E. E.; Jiao, C.; Wiley,  
577 L. A.; Mullins, R. F.; Stone, E. M.; et al. Effect of Molecular Weight and Functionality on Acrylated  
578 Poly(Caprolactone) for Stereolithography and Biomedical Applications. *Biomacromolecules* **2018**, 19 (9),  
579 3682–3692. <https://doi.org/10.1021/acs.biomac.8b00784>.
- 580 (54) Woodruff, M. A.; Hutmacher, D. W. The Return of a Forgotten Polymer - Polycaprolactone in the 21st  
581 Century. *Prog. Polym. Sci.* **2010**, 35 (10), 1217–1256.  
582 <https://doi.org/10.1016/j.progpolymsci.2010.04.002>.
- 583 (55) Busby, W.; Cameron, N. R.; Jahoda, C. A. B. Emulsion-Derived Foams (PolyHIPEs) Containing Poly( $\epsilon$ -  
584 Caprolactone) as Matrixes for Tissue Engineering. *Biomacromolecules* **2001**, 2 (1), 154–164.  
585 <https://doi.org/10.1021/bm0000889>.
- 586 (56) Lumelsky, Y.; Lalush-Michael, I.; Levenberg, S.; Silverstein, M. S. A Degradable, Porous, Emulsion-  
587 Templated Polyacrylate. *J. Polym. Sci. Part A Polym. Chem.* **2009**, 47 (24), 7043–7053.  
588 <https://doi.org/10.1002/pola.23744>.
- 589 (57) Lumelsky, Y.; Silverstein, M. S. Biodegradable Porous Polymers through Emulsion Templating.  
590 *Macromolecules* **2009**, 42 (5), 1627–1633. <https://doi.org/10.1021/ma802461m>.
- 591 (58) Pérez-García, M. G.; Gutiérrez, M. C.; Mota-Morales, J. D.; Luna-Bárcenas, G.; Del Monte, F. Synthesis of  
592 Biodegradable Macroporous Poly(l -Lactide)/Poly( $\epsilon$ -Caprolactone) Blend Using Oil-in-Eutectic-Mixture  
593 High-Internal-Phase Emulsions as Template. *ACS Appl. Mater. Interfaces* **2016**, 8 (26), 16939–16949.  
594 <https://doi.org/10.1021/acsami.6b04830>.

- 595 (59) Yang, X.; Yin, Z.; Zhang, X.; Zhu, Y.; Zhang, S. Fabrication of Emulsion-Templated Macroporous Poly( $\epsilon$ -  
596 Caprolactone) towards Highly Effective and Sustainable Oil/Water Separation. *Polymer (Guildf)*. **2020**,  
597 204. <https://doi.org/10.1016/j.polymer.2020.122852>.
- 598 (60) Yadav, A.; Pal, J.; Nandan, B.; Srivastava, R. K. Macroporous Scaffolds of Cross-Linked Poly( $\epsilon$ -  
599 Caprolactone) via High Internal Phase Emulsion Templating. *Polymer (Guildf)*. **2019**, 176, 66–73.  
600 <https://doi.org/10.1016/j.polymer.2019.05.034>.
- 601 (61) David, D.; Silverstein, M. S. Porous Polyurethanes Synthesized within High Internal Phase Emulsions. *J.*  
602 *Polym. Sci. Part A Polym. Chem.* **2009**, 47 (21), 5806–5814. <https://doi.org/10.1002/pola.23624>.
- 603 (62) Changotade, S.; Radu Bostan, G.; Consalus, A.; Poirier, F.; Peltzer, J.; Lataillade, J. J.; Lutomski, D.;  
604 Rohman, G. Preliminary in Vitro Assessment of Stem Cell Compatibility with Cross-Linked Poly( $\epsilon$  -  
605 Caprolactone Urethane) Scaffolds Designed through High Internal Phase Emulsions. *Stem Cells Int.* **2015**.  
606 <https://doi.org/10.1155/2015/283796>.
- 607 (63) Field, J.; Haycock, J. W.; Boissonade, F. M.; Claeysens, F. A Tuneable, Photocurable, Poly(Caprolactone)-  
608 Based Resin for Tissue Engineering—Synthesis, Characterisation and Use in Stereolithography. *Molecules* **2021**, 26 (5), 1199. <https://doi.org/10.3390/molecules26051199>.
- 610 (64) Han, S. B.; Kim, J. K.; Lee, G.; Kim, D. H. Mechanical Properties of Materials for Stem Cell Differentiation.  
611 *Adv. Biosyst.* **2020**, 4 (11). <https://doi.org/10.1002/adbi.202000247>.
- 612 (65) Hah, J.; Kim, D.-H. Deciphering Nuclear Mechanobiology in Laminopathy. *Cells* **2019**, 8 (3).  
613 <https://doi.org/10.3390/cells8030231>.
- 614 (66) Narasimhan, B. N.; Ting, M. S.; Kollmetz, T.; Horrocks, M. S.; Chalard, A. E.; Malmström, J. Mechanical  
615 Characterization for Cellular Mechanobiology: Current Trends and Future Prospects. *Frontiers in*  
616 *Bioengineering and Biotechnology*. 2020. <https://doi.org/10.3389/fbioe.2020.595978>.
- 617 (67) Kida, T.; Tanaka, R.; Nitta, K. H.; Shiono, T. Effect of the Number of Arms on the Mechanical Properties  
618 of a Star-Shaped Cyclic Olefin Copolymer. *Polym. Chem.* **2019**, 10 (41).  
619 <https://doi.org/10.1039/c9py01186b>.
- 620 (68) Doganci, M. D. Effects of Star-Shaped PCL Having Different Numbers of Arms on the Mechanical,  
621 Morphological, and Thermal Properties of PLA/PCL Blends. *J. Polym. Res.* **2021**, 28 (1).  
622 <https://doi.org/10.1007/s10965-020-02380-2>.
- 623 (69) Wang, S.; Kempen, D. H.; Simha, N. K.; Lewis, J. L.; Windebank, A. J.; Yaszemski, M. J.; Lu, L. Photo-Cross-  
624 Linked Hybrid Polymer Networks Consisting of Poly(Propylene Fumarate) and Poly(Caprolactone  
625 Fumarate): Controlled Physical Properties and Regulated Bone and Nerve Cell Responses.  
626 *Biomacromolecules* **2008**. <https://doi.org/10.1021/bm7012313>.
- 627 (70) Tian, G.; Zhu, G.; Ren, T.; Liu, Y.; Wei, K.; Liu, Y. X. The Effects of PCL Diol Molecular Weight on Properties  
628 of Shape Memory Poly( $\epsilon$ -Caprolactone) Networks. *J. Appl. Polym. Sci.* **2019**, 136 (6).  
629 <https://doi.org/10.1002/app.47055>.
- 630 (71) Peponi, L.; Navarro-Baena, I.; Báez, J. E.; Kenny, J. M.; Marcos-Fernández, A. Effect of the Molecular  
631 Weight on the Crystallinity of PCL-b-PLLA Di-Block Copolymers. *Polymer (Guildf)*. **2012**, 53 (21).  
632 <https://doi.org/10.1016/j.polymer.2012.07.066>.
- 633 (72) Wang, S.; Yaszemski, M. J.; Gruetzmacher, J. A.; Lu, L. Photo-Crosslinked Poly( $\epsilon$ -Caprolactone Fumarate)  
634 Networks: Roles of Crystallinity and Crosslinking Density in Determining Mechanical Properties. *Polymer*  
635 *(Guildf)*. **2008**, 49 (26). <https://doi.org/10.1016/j.polymer.2008.10.021>.
- 636 (73) Paterson, T. E.; Gigliobianco, G.; Sherborne, C.; Green, N. H.; Dugan, J. M.; MacNeil, S.; Reilly, G. C.;

637 Claeysens, F. Porous Microspheres Support Mesenchymal Progenitor Cell Ingrowth and Stimulate  
638 Angiogenesis. *APL Bioeng.* **2018**, 2 (2), 026103. <https://doi.org/10.1063/1.5008556>.

639 (74) Moglia, R. S.; Holm, J. L.; Sears, N. A.; Wilson, C. J.; Harrison, D. M.; Cosgriff-Hernandez, E. Injectable  
640 PolyHIPEs as High-Porosity Bone Grafts. *Biomacromolecules* **2011**, 12 (10), 3621–3628.  
641 <https://doi.org/10.1021/bm2008839>.

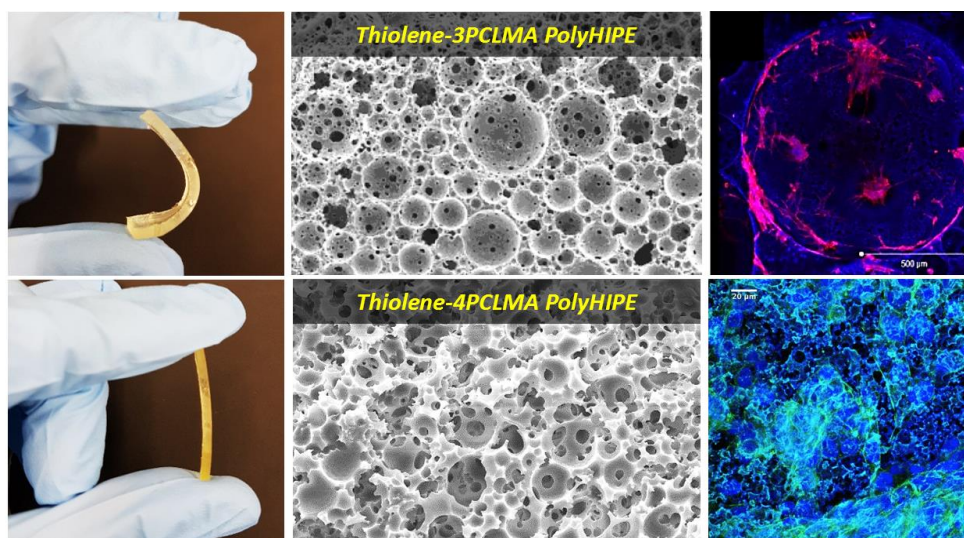
642 (75) Grosvenor, M. P.; Staniforth, J. N. The Effect of Molecular Weight on the Rheological and Tensile  
643 Properties of Poly( $\epsilon$ -Caprolactone). *Int. J. Pharm.* **1996**, 135 (1–2). [https://doi.org/10.1016/0378-5173\(95\)04404-3](https://doi.org/10.1016/0378-5173(95)04404-3).  
644

645 (76) Aslantürk, Ö. S. In Vitro Cytotoxicity and Cell Viability Assays: Principles, Advantages, and Disadvantages.  
646 In *Genotoxicity - A Predictable Risk to Our Actual World*; InTech, 2018.  
647 <https://doi.org/10.5772/intechopen.71923>.

648

649

650 ***For Table of Contents Only***



651